

Fabrication of plasmonic Au nanovoid trench arrays by guided self-assembly

Xiaoli V Li¹, R M Cole², C A Milhano³, P N Bartlett³, B F Soares²,
J J Baumberg² and C H de Groot¹

(Ed:)

¹ School of Electronics and Computer Science, University of Southampton,
Southampton SO17 1BJ, UK

² Department of Physics, University of Cambridge, J J Thomson Avenue,
Cambridge CB3 0HE, UK

³ School of Chemistry, University of Southampton, Southampton SO17 1BJ, UK

E-mail: xl2@ecs.soton.ac.uk and rme59@cam.ac.uk

Received 27 March 2009, in final form 5 May 2009

Published

Online at stacks.iop.org/Nano/20/000000

Ascii/Word/NAN/
nano313708/PAP
Printed 26/5/2009
Spelling UK
Issue no
Total pages
First page
Last page
File name
Date req
Artnum
Cover date

Abstract

Metallic nanoscale voids can support both localized and propagating plasmons and form plasmonic crystals. However, constructing 1D arrays is crucial for producing plasmonic circuits. In this paper we report the first experimental evidence of plasmons in templated linear arrays of self-assembled structures. Single and multilayer arrays of gold voids have been fabricated through self-assembly of sub-micron polystyrene spheres in V-shaped trenches in silicon, followed by selective area electrodeposition. Angle-dependent dispersion characteristics reveal the existence of localized plasmons.

- Q.1** fabricated through self-assembly of sub-micron polystyrene spheres in V-shaped trenches in silicon, followed by selective area electrodeposition. Angle-dependent dispersion characteristics reveal the existence of localized plasmons.
- Q.2** (Some figures in this article are in colour only in the electronic version)

1. Introduction

Plasmonic devices rely on the interaction of light with free charges, and are key to optical sensing and waveguiding [1]. High quality three-dimensional colloidal sphere arrays have attracted attention due to their potential to act as a template for the fabrication of 3D photonic crystals for waveguide structures, optical filters or switches [2]. In previous work [3, 4], we have shown that spherical nanoscale voids in metal possess different, and potentially more useful, plasmonic modes than nanoscale metal particles. In particular, it has been shown that spherical nanoscale voids, fabricated using a substrate of hexagonal close-packed self-assembled spheres as a template, support both propagating and localized plasmon modes, as shown in figure 1 [3, 4]. In 2D nanovoid arrays the incident energy spreads out rapidly and pulses disperse in many directions, while on the other hand in linear chains of nanovoids propagation can be very low loss and non-dispersive. This compares to nanoparticle plasmon chains which quench propagation after only one or two interparticle hops. Only by making linear arrays of such nanovoid structures is it possible to guide plasmons in specific geometric directions and fabricate plasmon waveguides which will enable on-chip optical communication. However, previously it has not been possible to control the direction of plasmon propagation.

Patterned or guided assembly of a few micron or sub-micron sized particles has recently attracted a lot of attention, and assembly of various kinds of particles in trenches and holes has been demonstrated. This method allows the formation of shapes of a size which is at least an order of magnitude smaller than that of the pattern made by (photo-) lithography or other means. Cheng *et al* succeeded in regular assembly of block co-polymers of 50 nm period [5, 6] which is particularly useful for high density storage [7]. However, for optical interactions, particle sizes of the order of visible light wavelengths are required. Ozin *et al* have shown both theoretically and experimentally the optical absorption spectra of self-assembled polystyrene spheres on patterned silicon [8, 9] as have Sun *et al* on polycarbonate substrates [10]. Whispering gallery modes have been detected in one-dimensional arrays of self-assembled spheres by Hara *et al* [11] although in this experiment the polymer spheres had to be selected spectroscopically to reduce the sphere to sphere size variation.

Mono-dispersed spherical colloids can self-assemble into one, two, or three-dimensional lattices [12–14] by various types of driving forces, such as gravity, convection, spin-coating or electrostatics [15–18]. On flat substrates, spheres self-assemble due to capillary forces into hexagonal close-packed mono- or multi-layers, as a maximum packing density

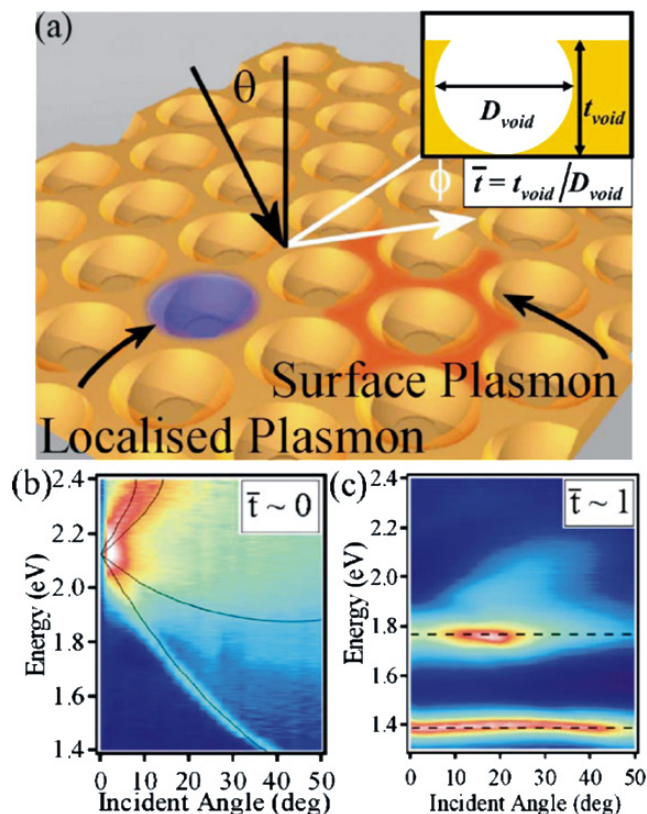


Figure 1. (a) Schematic of surface plasmons (blue, in colour on-line) and localized plasmons (red) existing on gold nanoscale void surfaces. θ is the angle of incidence with respect to the normal, and Φ the angle with respect to the hexagonal lattice director. ((b), (c)) Typical experimental angle-dependent plasmon dispersions, with absorption from 0% (dark blue) to 80% (red/white), for (b) a propagating surface plasmon (black lines indicate theoretical dispersion modelled using the Bragg scattering equation), and (c) a localized plasmon (dashed lines indicate expected plasmon energy). Existence of the different plasmons depends on the thickness of the Au. See [3] for details.

Q.A

is the energetically favourable structure. However, on patterned substrates, the main packing force is the surface interactions between the spheres and the walls of the template. Therefore the packing structure of spheres on a patterned substrate is primarily directed by local physical constraints, as shown in [19–28].

In this paper, we use self-assembly of polystyrene spheres on patterned substrates to create a template for the electrodeposition of Au nanoscale void arrays. Sphere assembly in flat bottomed trenches has previously been demonstrated by Conway *et al* [29] and Woodcock [30], however here we use V-shaped trenches and show how the observed ordered crystal stacking is uniquely controlled in this configuration. The diameter of the polystyrene spheres and hence the size of Au voids is around 500 nm, which allows us to probe both self-assembly formation and plasmon modes with visible light. The quality and fidelity of both the self-assembly of polystyrene spheres as well as the electrodeposition of Au nanovoids is such that we have been able to detect the existence of localized plasmons by optical means. The energy of the plasmons is shown to depend on the dielectric constant at the

Au interface. This is the first experimental evidence of linear plasmon arrays in templated self-assembled structures.

2. Experimental section

The templates were assembled using mono-disperse polystyrene polystyrene spheres (Duke Scientific Corporation) supplied as a 1 wt% solution in water (manufacturer's certified mean diameter of $499 \text{ nm} \pm 5 \text{ nm}$, coefficient of variation in diameter 1.3%). Before use the suspensions were homogenized by successive, gentle inversions for 5 min followed by a sonication for 15 s. All solvents and chemicals were of reagent quality and were used without further purification. The commercial cyanide free gold plating solution (Tech. Gold 25, containing 7.07 g dm^{-3} gold) was obtained from Technic Inc. (Cranston, RI, USA). Fuming nitric acid and dimethylformamide (DMF) was obtained from Aldrich. 20:1 buffered hydrogen fluoride (BHF) was obtained from Rockwood. All solutions were freshly prepared using reagent-grade water ($18 \text{ M}\Omega \text{ cm}$) from a Cartridge Elga deioniser system.

The pre-patterned Si substrates were prepared from n-type (100)-polished Si substrate wafers with $0.01\text{--}0.02 \text{ }\Omega \text{ cm}$ resistivity. The process flow for the samples is outlined in figure 2. A 250 nm layer of SiO_2 was thermally grown. A photolithography pattern was then transferred onto the wafer surface and the oxide was dry etched down to the underlying Si, creating linear trench arrays of $400 \text{ }\mu\text{m}$ length, with widths W varying from 500 to 1700 nm with a step size of 100 nm and separation between the strips of either 500 or 1000 nm. To obtain V-shaped trenches, Si wet etching by potassium hydroxide (KOH) was carried out, (figure 2(b)). This intrinsically anisotropic etching technique utilizes a relative etch rate for (111)/(100) Si planes of about 350 [18]. Therefore orientation-dependent etching of (100)-polished Si through the patterned SiO_2 mask creates precise V-shaped trenches, with an angle of 70.6° between two (111)-planes. Wafers are cleaned using a two-step RCA clean, with an aqueous mixture of hydrogen peroxide and ammonium hydroxide and a mixture of hydrogen peroxide and hydrochloric acid. Prior to the deposition of spheres, a 20:1 BHF dip is used to etch the native oxide layer off the exposed Si. In order to assemble the colloidal spheres on the patterned Si wafer, a clean uncoated microscope slide was attached to the wafer forming a water-tight cell. A layer of Parafilm was used to prevent the leakage from the cell, and a hatch was left to allow the injection of the colloidal solution. The cell was clamped vertically and the solution allowed to evaporate naturally over 10 h, enabling assembly of the spheres in the trenches, as shown in figure 2(c). Prior to electrodeposition, a second 20:1 BHF dip (6 s) was necessary to remove the native oxide and leave the Si surface H-terminated. Electrodeposition of gold was then performed at ambient temperature using a conventional three-electrode configuration controlled by an Autolab PGSTAT12. The sample was the working electrode with a platinum gauze counter electrode and a saturated calomel reference electrode (SCE). A pulse of -1.1 V versus SCE was applied for 0.2 s to nucleate electrodeposition. The gold nanoscale voids were gradually electrodeposited under potentiostatic

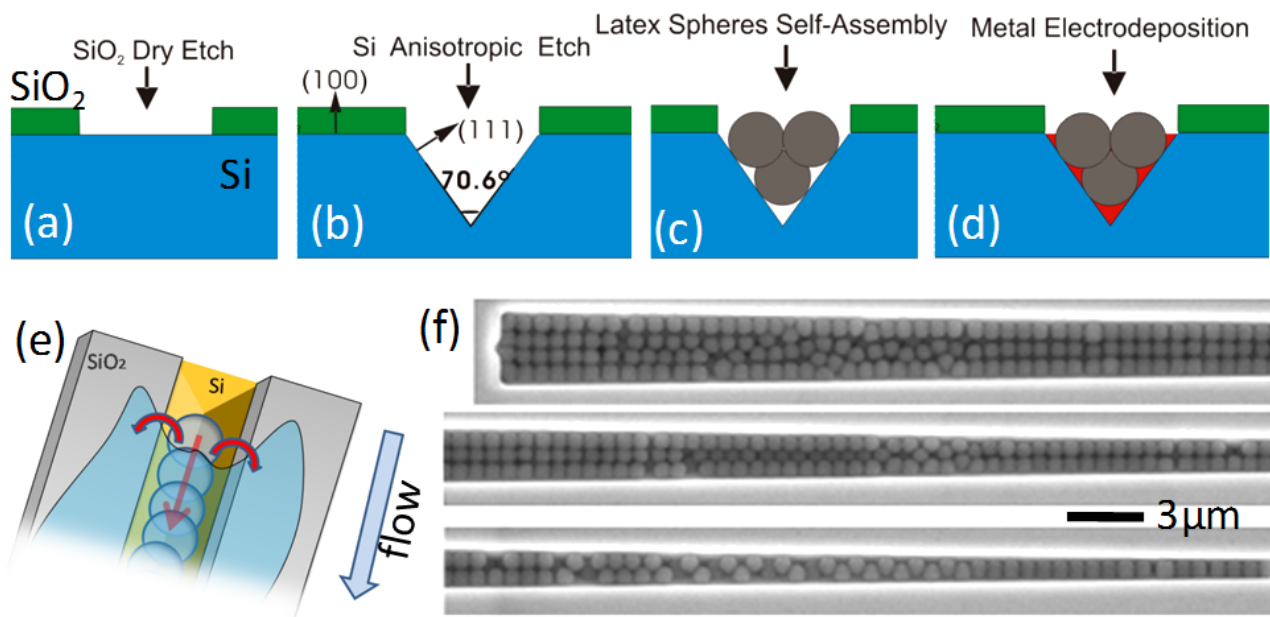


Figure 2. ((a)–(d)) Process flow and schematic view for templated self-assembly of inverse sphere metal arrays in V-shaped trenches: (a) SiO₂ dry etch by hydrofluoric acid through a lithographically patterned photo-resist layer (not shown) (b) Si anisotropic etch by potassium hydroxide (c) self-assembly of polystyrene spheres by solvent evaporation (d) Au electrodeposition on Si through the polystyrene template. (e) The water preferentially wets the SiO₂ thus forcing the spheres along the trench into contact. (f) Sequential SEM images of 600 nm colloidal spheres assembled in a 3D lattice inside a tapered trench of length 75 μm, width from 2500 nm (top left) to 560 nm (bottom right).

conditions at -0.7 V versus SCE. Since SiO₂ is an insulator, electrodeposition only takes place on the Si trench walls, as shown in figure 2(d). After electrodeposition, the sample was placed into dimethylformamide (DMF) solvent and washed in an ultrasonic tank for 2 h in order to dissolve the polystyrene sphere template. The morphology and nanostructure of both the colloidal templates and gold nanoscale void arrays were characterized using scanning electron microscopy (SEM, LEO 1455VP SEM). A fibre-coupled spectrometer (Ocean Optics, spectral range 400–1700 nm, resolution 1 nm) placed in the focal plane of the reflection image was used to obtain the spectral response from the selected area (approximate diameter 50 μm).

3. Results and discussion

3.1. Templated self-assembly of colloidal spheres

Polystyrene spheres assembled in the V-shaped trenches, are first characterized by SEM. Spheres with diameter $D_n = 500$ nm, can be seen assembled three-dimensionally in a trench of nominal width $W_n = 1800$ nm in figure 3(a). From the right most trench in the SEM image in which the layer below the top layer is revealed, it is clear that the spheres assemble in a face centred cubic (fcc) lattice with the (001) plane in the plane of the wafer and the (110) direction parallel to the trench length and the Si (110) direction. The number of spheres observed in the top layer perpendicular to the trench corresponds to the number of dense packed planes of the colloidal crystal within the V-shaped trenches. The angle in the shown fcc stacking of the spheres with its (111) plane parallel to the crystal Si (111) planes means that the fcc polystyrene sphere lattice has

an identical angle to the horizontal plane as the Si. The (111) packing of the sphere lattice forms hence parallel to the trench angled sidewalls, maximizing the number of spheres touching the Si wall. Hence fcc is the closest-packed arrangement in a KOH etch Si trench when the trench width is commensurate with the sphere size. This is in contrast to flat bottom structures in which the hexagonal lattice is instead favoured for a single layer [29, 30], which will build up to a fcc lattice with the (111) plane in the *plane* of the wafer as shown in [31]. The orientation of the assembled structure is hence predictably controlled by the geometry of the trench.

The most dense ordered packing is expected for a commensurate trench size with the width W of the trench equal to $W = nD + A$ with n the integer identical to the number of layers, and A an offset due to spheres not being able to access the bottom apex of the V-grooved trench. However, as nothing would stop the spheres partially assembling in the anisotropically etched SiO₂ above the Si, the effective offset can be essentially zero. Although there is some fluctuation, experimentally for sphere diameter $D = 500$ nm, the four-layer structure assembles most repeatably in a trench of measured width $W_n = 2130$ nm, the three-layer structure in $W_n = 1580$ nm, the two layer in $W_n = 1020$ nm, and the one layer in $W_n = 470$ nm as shown in figure 3. The relation between experimental width and sphere diameter for commensurate structures hence fits closely the relation $W_e = nD$ with the data suggesting that for wider structures it needs to be slightly larger than the commensurate size to accommodate both the variation in sphere size (1.3%) and aligned movement as the fcc phase forms.

It is also worth noting that the polystyrene spheres do not assemble on SiO₂ surfaces in the vicinity of the Si trenches. On

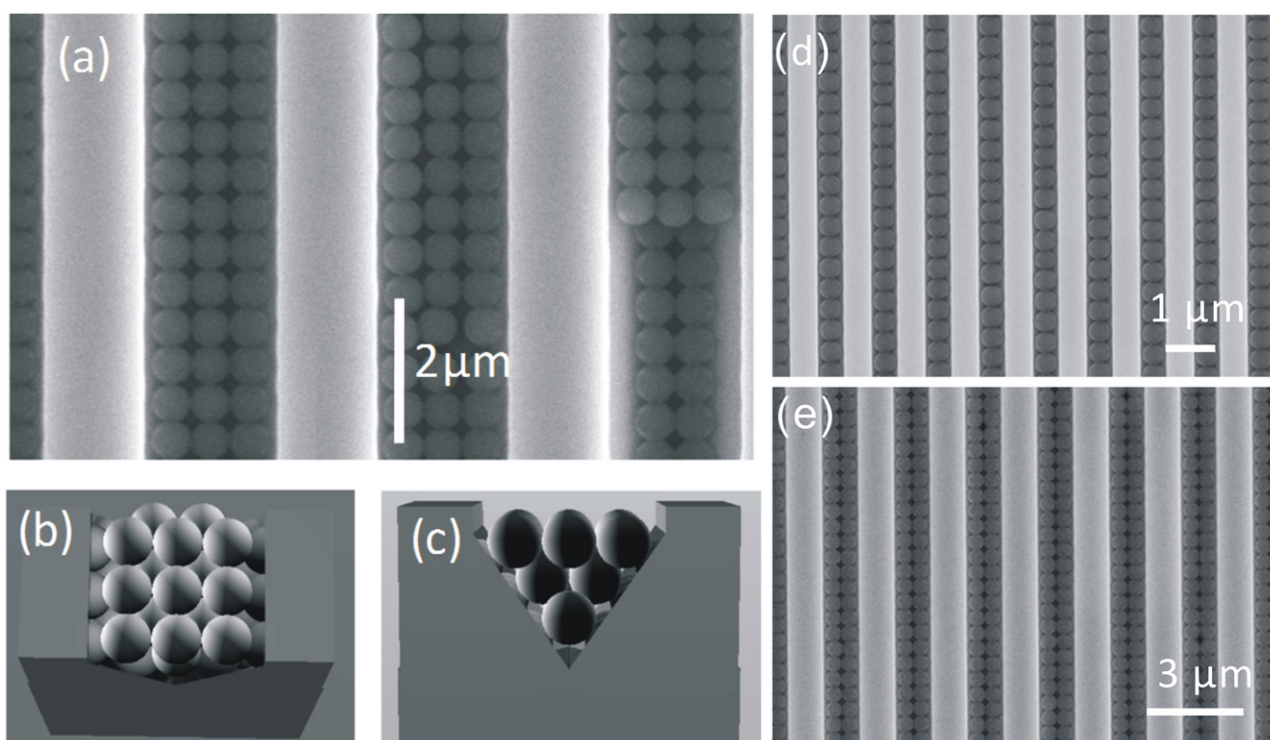


Figure 3. SEM images of 500 nm polystyrene sphere arrays that were assembled into trenches by controlled evaporation of water. In (a) with 1580 nm trench width, the first sub-layer is exposed in the bottom right-hand side revealing the fcc lattice, with schematic (b) top view and (c) cross-sectional view of the self-assembled lattice. Trenches of width (d) 470 nm and (e) 1020 nm support single and double layers of spheres respectively.

un-patterned planar Si or SiO₂ surfaces, polystyrene spheres assemble into a close-packed array driven by strong lateral capillary forces [32], which develop at the meniscus between the solution and substrate and between adjacent spheres. In contrast, on the patterned Si wafer, the mechanism of self-assembly is altered as competing surface energies play a role. The buffered hydrogen fluoride dip used on the Si surface before self-assembly leaves the surface H-terminated, and thus hydrophobic. Hence it is expected that the SiO₂ has a smaller contact angle and higher surface energy than the Si surface. The liquid better wets the SiO₂ thus retracting from the Si trenches first and is only retained in the vicinity of the polystyrene spheres which are lifted up to the rim edge and brought into contact with the previously deposited spheres (see figure 2(e)). The combination of maximizing electrostatic attraction between the spheres and the Si trench sidewalls, and the capillary forces developed by the different wetting of trench and rim appears to guarantee dense ordered packing in this system. This close-packed geometry is critical for the subsequent fabrication of Au nanovoid linear arrays since the touching spheres produce eventually interconnecting holes between the voids that control the hopping of localized plasmons along the chain [3].

3.2. Optical characteristics of patterned and self-assembled structures

Un-patterned Si wafers appear dark grey in dark field microscopy. The intrinsic colouration of the wafers seen in

figure 4 is due to optical diffraction from the periodic micro patterning of the surface. Unfilled trenches of nominal widths from 500 to 1200 nm were imaged in dark field configuration, as shown in figure 4(a). In dark field imaging, light impinges at higher angles (10°) and only scattered (i.e. diffracted) light at normal incidence is collected by the objective, as in figure 4(c). A simple calculation of the peak diffracted wavelengths as a function of trench pitch shows excellent agreement with the microscope image colours (figure 4(d)), providing a rapid method to verify the trench pitch and substrate uniformity at precise locations. Figure 4(b) shows an equivalent substrate with spheres assembled into the trenches. The spheres modify the local refractive index, tuning the effective pitch of the trenches, and hence tuning their colour. From the uniformity of trench array colour, the sphere packing density can be measured, as observed in figure 4(e) for samples of increasing sphere concentration in the trenches. Well-ordered samples with good adhesion to the patterned substrate appear opalescent.

3.3. Gold electrodeposition through colloidal sphere template

After self-assembly, the 3D lattices are used as templates to fabricate Au nanoscale void arrays on Si by electrodeposition. A pulse of -1.1 V versus SCE for 0.2 s is used to form a layer of uniform Au nucleation as with Si as the electrodeposition interface, instantaneous uniform nucleation is crucial to obtain a continuous gold film [33]. A potential of -0.7 V versus SCE was selected to allow the gradual electrodeposition of Au

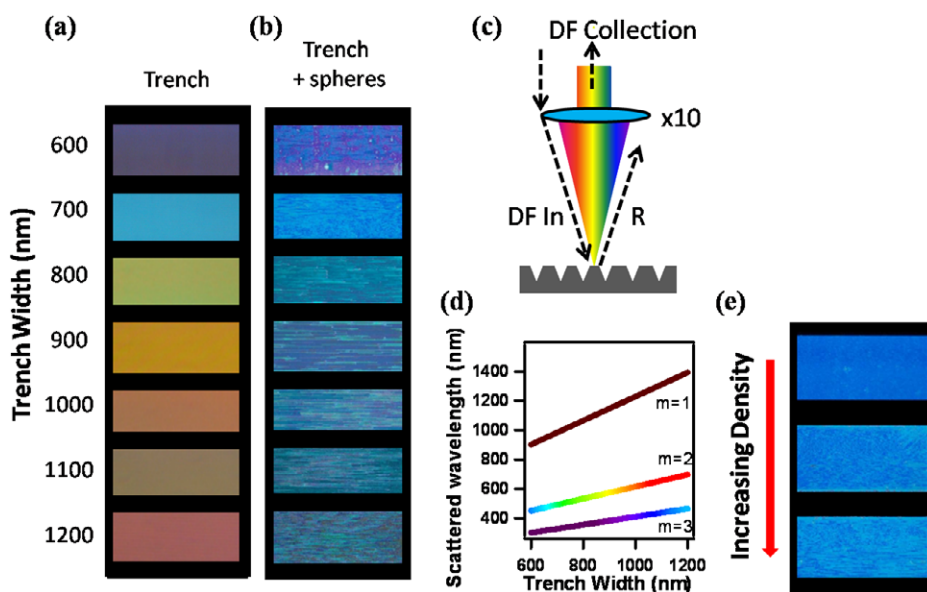


Figure 4. Dark field microscope images of 250 μm -long trench arrays with width varying step-wise from 600 to 1200 nm and fixed spacing between trenches of 500 nm, either (a) empty or (b) filled with self-assembled polystyrene sphere. Colour changes across each filled trench array are due to changes in the local refractive index, which is directly related to the sphere packing density and uniformity. (c) Schematic of light collection by microscope in dark field configuration. (d) Calculated diffracted wavelengths for the three lowest diffraction orders as a function of trench width, with appropriate corresponding colours (on-line). (e) Dark field microscope images of trench arrays with increasing density of polystyrene spheres. Sphere packing density can be inferred from each image.

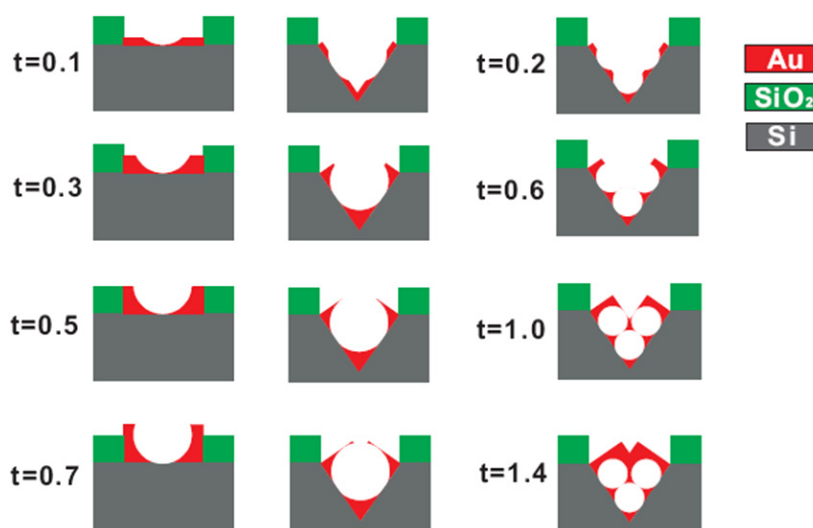


Figure 5. Electrochemical growth of Au around sphere templates in rectangular and V-groove trenches, showing the enhanced encapsulation rate in V-grooves for similar charge passed.

without any further nucleation. As shown in figure 6, using 500 nm diameter colloidal spheres chains, single line spherical nanoscale voids arrays of Au are grown in the 560 nm trenches whilst double line void arrays of Au are grown in 1300 nm trenches. As electrodeposition requires a conductive substrate, Au electrodeposition occurs only on the Si surface and not on the top insulating SiO₂, resulting in confinement of the metal arrays exclusively to the Si trenches, independently of whether polystyrene spheres have assembled on the SiO₂.

Gold growth begins simultaneously from both walls of the V-shaped trenches, where Si has a (111) orientation (figure 5). The volume of the gold deposited is linearly related to the

charge passed through the electrodes during electrodeposition and is hence well controlled. However, compared with nanoscale voids grown on a flat substrate, the structure of the Au grown into V-shaped groove trenches is more complicated: due to the V-shaped geometry, gold growth is most rapid at the bottom apex of the trench. A range of structures from shallow dishes, to triangular islands and truncated spherical cavities can be fabricated depending on the volume of Au deposited. For a given electrodeposition volume, the void shapes in the V-shaped trenches form deeper cavities than those on flat bottom trenches leading to faster encapsulation of the spheres. After Au deposition, the spheres can be dissolved, leaving a highly

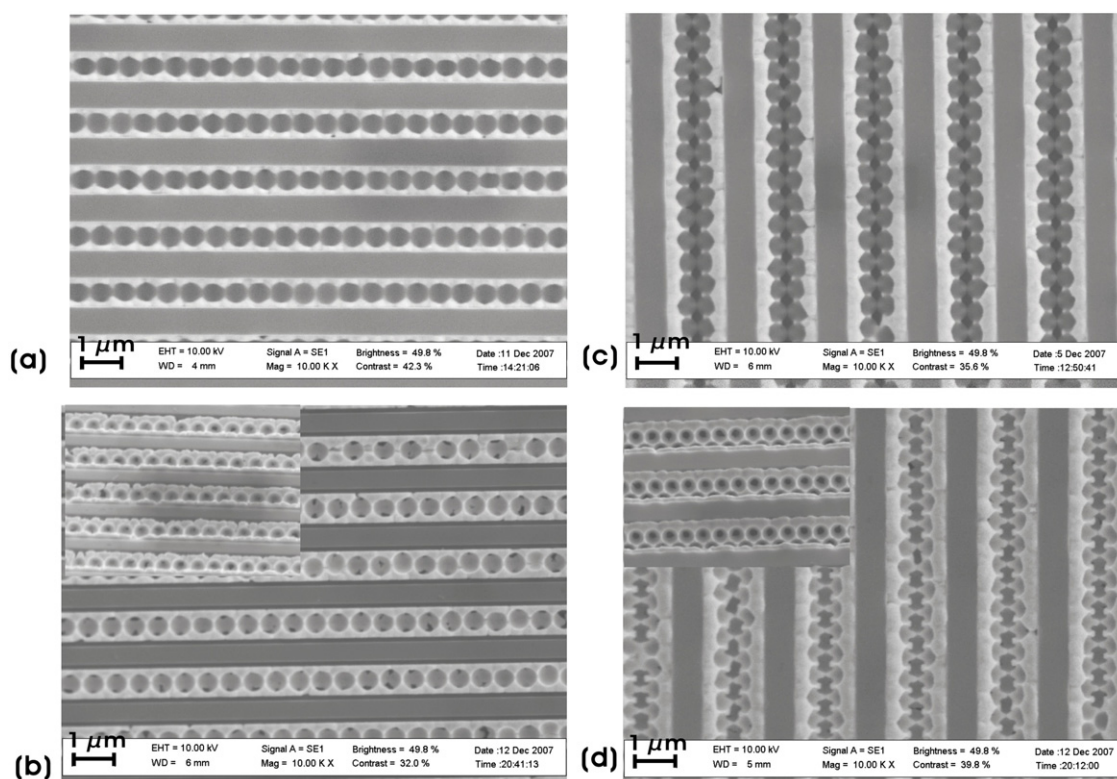


Figure 6. SEM images of 500 nm nanoscale void arrays. The voids are grown by Au electrodeposition using the assembled polystyrene linear sphere arrays as templates. ((a), (b)) Single nanovoid arrays in trenches of width 560 nm with (a) polystyrene spheres present or (b) dissolved. ((c), (d)) Double nanovoid arrays in trenches of width 1300 nm with polystyrene spheres (c) present or (d) dissolved. The insets show the view of the structure tilted at a 45° angle.

stable Au nanovoid morphology. Such isolated plasmon array 3D structures have not previously been fabricated, and are hard to conceive of using alternative routes.

3.4. Optical characteristics of gold nanovoids

Angle-dependent optical characterization of these structures reveals a rich variety of optical and plasmonic modes, which are strongly dependent on the lattice structure and Au thickness. Angular-dispersion measurements can reveal the nature of the observed plasmon modes, as depicted in figure 1. Optical reflectivity measurements for two different samples are shown in figure 7. The samples were illuminated with visible light from 400 to 1700 nm, and incident scan angles from 0° to 80°. The thickness ratio t/D is 0.5 for the upper sphere in each structure, corresponding to a semi-truncated spherical cavity. First we identify weak but highly dispersive (i.e. strongly angle dependent) modes which correspond to propagating plasmon modes on the top of the Au (solid line in figure 7(a)), where the plasmon frequency depends on the incident photon wavevector. The dispersion of these modes corresponds to plasmons propagating along the length of the trenches. These modes disappear when the sample is oriented so the incident light is oriented not along, but across the nanovoid trench arrays, as such plasmons can no longer propagate (figure 8(a)). We note also that the plasmonic absorption in our linear nanovoid array devices is less pronounced than on un-patterned 2D array substrates, due to the reduced nanovoid density.

The data also reveals highly localized modes (dashed lines), which due to their confined spatial extent, have a well defined plasmon frequency across a wider angular range. These modes are characterized by a flat dispersion, and are predominant in high aspect ratio nanoscale void structures. Hopping of localized plasmons between neighbouring spheres can be identified from the presence of ‘nearly’ localized plasmons with mixed Bragg–Mie dispersion (figure 8(b))—these plasmon bands weakly disperse and show anti-crossing behaviour where they meet. Whereas light incident on a 2D hexagonal nanoscale void array can couple to plasmon modes at any incident azimuthal angle to the crystal lattice, in the trench structures only light incident parallel to the trenches will couple strongly to plasmon modes, with only weak coupling to localized plasmons by light incident perpendicular to the trenches. This highlights the crucial role of the trenches in guiding and confining the propagating plasmons.

Both the localized modes and dispersive modes are better defined with the colloidal spheres left in place (providing a high refractive core confining the plasmons better). It can also be seen that the localized plasmon present in the single-layer structure (figure 7(a), red arrow) shifts to higher energy when the spheres are removed (figure 7(b)). This is a direct consequence of the lower dielectric constant of the air as compared to the colloidal spheres, as described in detail in [34]. In addition, the plasmon linewidths are broader when the spheres are removed (more than doubling the linewidth) due

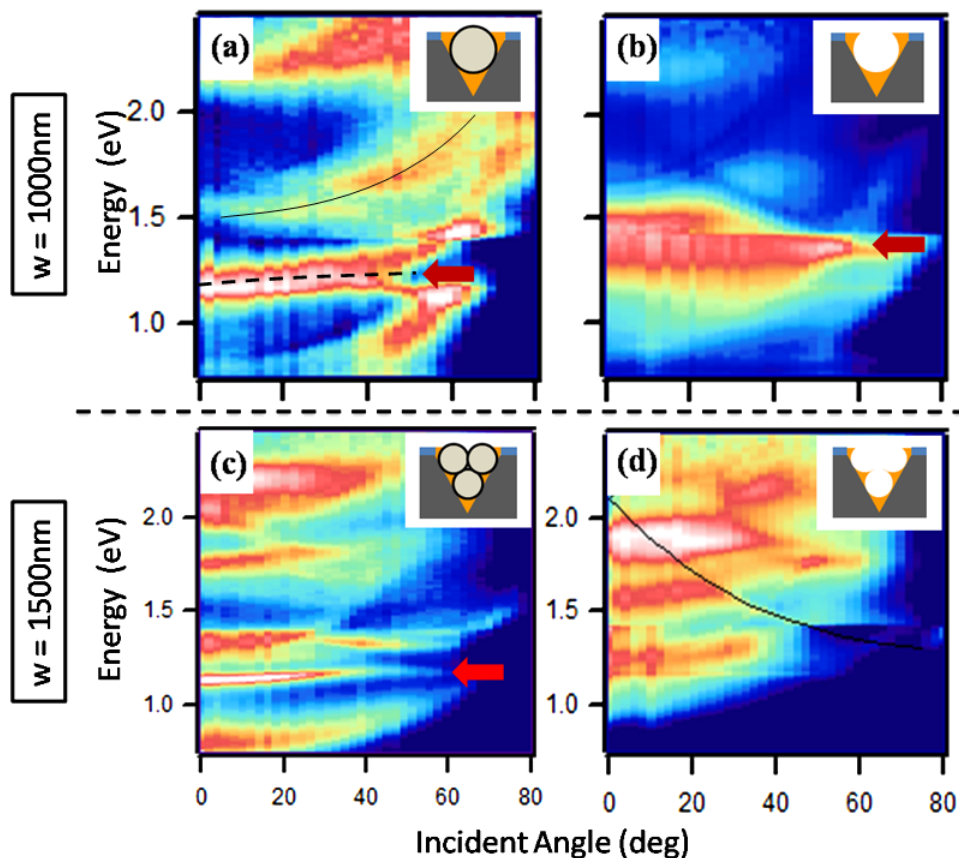


Figure 7. Angle-dependent dispersion of plasmon absorption from $\alpha = 0\%$ (dark blue) to $\alpha = 80\%$ (white). Single-((a), (b)) and double-((c), (d)) layer 500 nm diameter nanoscale Au voids electrodeposited in trenches of width 840 nm with the polystyrene spheres present ((a), (c)) or dissolved ((b), (d)). Arrows identify a localized plasmon whose energy blue-shifts when the spheres are removed. Black line shows the theoretical dispersion of a plasmon propagating along the flat metal above the voids.

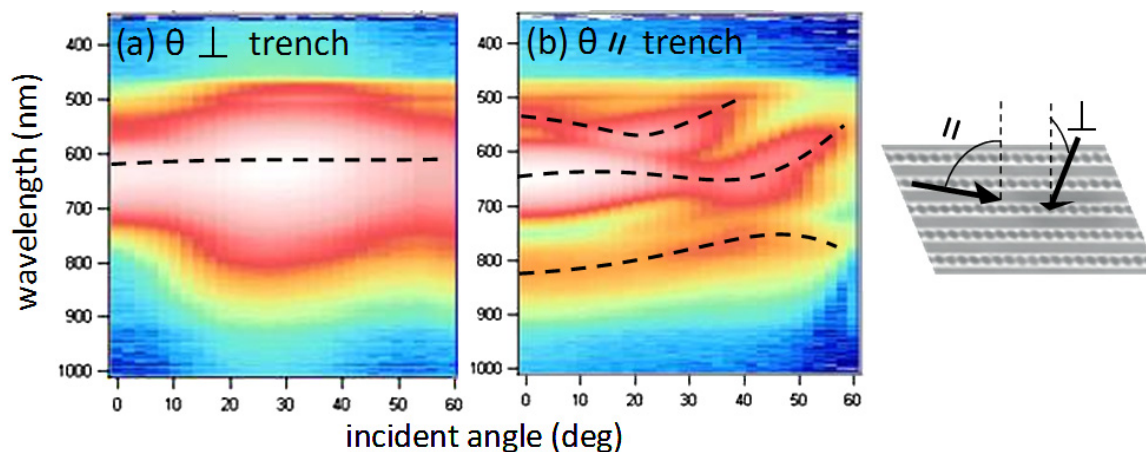


Figure 8. Angle-dependent dispersion of plasmon absorption for light incident (a) across and (b) along the line of the trenches of Au nanovoids of diameter 500 nm in 1490 nm wide trenches. Plasmons (dashed lines to guide eye) do not couple across trenches (flat line), but do propagate along nanovoids.

to the increased radiative decay of the plasmons without the high refractive index sphere in the core of the nanovoid.

Further theoretical work to understand the nature of localized plasmon hopping between nanovoids (which sets the angular dispersion of the observed bands) is underway. However the data shown here clearly show the influence of the trench morphology on the plasmon dispersion.

4. Conclusions

We have demonstrated a method to fabricate gold nanoscale voids in linear arrays, capable of supporting plasmons. In this method photolithography is used to pre-pattern a Si surface, which is then selectively etched in KOH to create series of V-shape groove trenches. The geometric confinement of the

trenches together with electrostatic interactions and surface tension guides the (110) fcc assembly of the spheres on this patterned Si surface. Zero-defect arrays were found to assemble along the entire length of some trenches for 500 nm diameter spheres, allowing characterization with visible light. The long-range well-ordered sphere strip arrays are used as templates to form gold nanoscale void linear arrays by a carefully-developed electrodeposition process optimized for this architecture. By varying the film thickness, void shapes ranging from shallow dishes to encapsulated voids were fabricated. The gold nanovoid linear arrays are of high quality with respect to lateral symmetry and allow the detection of anisotropic plasmonic dispersion. Further understanding of the different plasmon modes will aid research into slow-light and active waveguides and potentially allow on-chip optical communication through nanovoid plasmon chains.

References

- [1] Lal S, Link S and Halas N J 2007 *Nat. Photon.* **1** 641
- [2] Wiley B J, Im S H, Li Z, McLellan J, Siekkinen A and Xia Y 2006 *J. Phys. Chem. B* **110** 15666
- [3] Kelf T A, Sugawara Y, Cole R M, Baumberg J J, Abdelsalam M E, Cintra S, Mahajan S, Russell A E and Bartlett P N 2006 *Phys. Rev. B* **74** 245415
- [4] Cole R M, Baumberg J J, Garcia de Abajo F J, Mahajan S, Abdelsalam M and Bartlett P N 2007 *Nano Lett.* **7** 2094
- [5] Cheng J Y, Ross C A, Thomas E L, Smith H I and Julius Vancso G 2003 *Adv. Mater.* **15** 1599
- [6] Cheng J Y, Mayes A M and Ross C A 2001 *Nat. Mater.* **3** 823
- [7] Park S, Lee D H, Xu J, Kim B, Hong S W, Jeong U, Xu T and Russell T P 2009 *Science* **323** 1030
- [8] Ozin G A and Yang S M 2001 *Adv. Funct. Mater.* **11** 95
- [9] Yang S M, Míguez H and Ozin G A *Adv. Funct. Mater.* **12** 425
- [10] Sun J, Li Y, Dong H, Zhan P, Tang C, Zhu M and Wang Z 2008 *Adv. Mater.* **20** 123
- [11] Hara Y, Mukaiyama T, Takeda K and Kuwata-Gonokami M 2005 *Phys. Rev. Lett.* **94** 203905
- [12] Bae C, Shin H and Moon J 2007 *Chem. Mater.* **19** 1531
- [13] Ye J, Zentel R, Arpiainen S, Ahopelto J, Jonsson F, Romanov S G and Sotomayor-Torres M C 2006 *Langmuir* **22** 7378
- [14] Nagayama K 1996 *Colloids Surf. A* **109** 363
- [15] Donselaar L N, Philipse A P and Suurmond J 1997 *Langmuir* **13** 6018
- [16] Denkov N D, Velev O D, Kralchevsky P A, Ivanov I B, Yoshimura H and Nagayama K 1992 *Langmuir* **8** 3183
- [17] Hulteen J C and van Duyne R P 1995 *J. Vac. Sci. Technol. A* **13** 1553
- [18] Kalsin A M, Fialkowski M, Paszewski M, Smoukov S K, Bishop K J M and Grzybowski B A 2006 *Science* **312** 420
- [19] van Blaaderen A, Ruel R and Wiltzius P 1997 *Nature* **385** 321
- [20] Kiziroglou M E, Li X, Gonzalez D C, de Groot C H, Zhukov A A, de Groot P A J and Bartlett P N 2006 *J. Appl. Phys.* **100** 113720
- [21] Ozin G A and Yang S M 2001 *Adv. Funct. Mater.* **11** 95
- [22] Yang S M and Ozin G A 2000 *Chem. Commun.* 2507
- [23] Yin Y D, Lu Y, Gates B and Xia Y 2001 *J. Am. Chem. Soc.* **123** 8718
- [24] Yin Y D, Li Z Y and Xia Y 2003 *Langmuir* **19** 622
- [25] Xia Y, Yin Y D, Lu Y and McLennan J 2003 *Adv. Funct. Mater.* **13** 907
- [26] WU S, Tang T and Tseng W J 2008 *J. Mater. Sci.* **43** 6453
- [27] Ye Y H, Badilescu S and Truong V 2001 *Appl. Phys. Lett.* **79** 872
- [28] Hur J and Won Y 2008 *Soft Matter* **4** 1261
- [29] Conway J H and Sloane N J A 1988 *Sphere Packings, Lattices and Groups* (New York: Springer)
- [30] Woodcock L V 1997 *Nature* **385** 141–3
- [31] Zhukov A A, Goncharov A V, de Groot P A J, Bartlett P N and Ghanem M A 2003 *J. Appl. Phys.* **93** 7322
- [32] Kralchevsky P A and Denkov N D 2001 *Curr. Opin. Colloid Interface Sci.* **6** 383
- [33] Kiziroglou M E, Zhukov A A, Li X, Gonzalez D C, de Groot P A J, Bartlett P N and de Groot C H 2006 *Solid State Commun.* **140** 508
- [34] Cole R M, Sugawara Y, Baumberg J J, Mahajan S, Abdelsalam M and Bartlett P N 2006 *Phys. Rev. Lett.* **97** 137401

Queries for IOP paper 313708

Journal: Nano

Author: X V Li et al

Short title: **Fabrication of plasmonic Au nanovoid trench arrays by guided self-assembly**

Page 1

Query 1:

Author: 'through guided' or 'by guided' better in title?

Query 2:

Author: Please be aware that the colour figures in this article will only appear in colour in the Web version. If you require colour in the printed journal and have not previously arranged it, please contact the Production Editor now.

Page 2

Query A:

Author: If figures 1, 4 and 7 are not to be printed in colour please provide alternatives for the colours mentioned in the captions.

Page 8

Query 3:-

Author: [9]: Please provide year.

Reference linking to the original articles

References with a volume and page number in blue have a clickable link to the original article created from data deposited by its publisher at CrossRef. Any anomalously unlinked references should be checked for accuracy. Pale purple is used for links to e-prints at ArXiv.